International Conference on Space Optics—ICSO 2010

Rhodes Island, Greece

4–8 October 2010

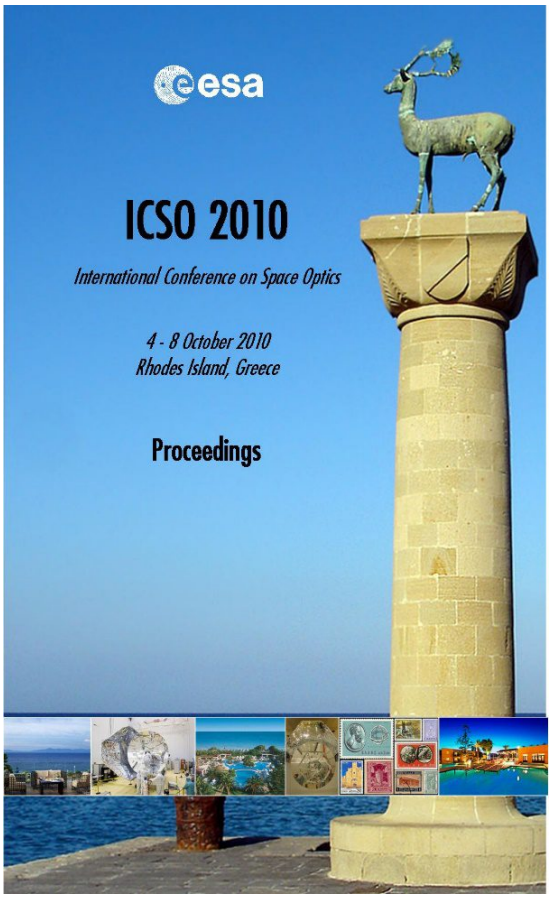

Edited by Errico Armandillo, Bruno Cugny, and Nikos Karafolas

Athermal fiber laser for the SWARM absolute scalar magnetometer

W. Fourcault, J.-M. Léger, V. Costes, I. Fratter, et al.

International Conference on Space Optics — ICSO 2010, edited by Errico Armandillo, Bruno Cugny, Nikos Karafolas, Proc. of SPIE Vol. 10565, 105650P · © 2010 ESA and CNES
CCC code: 0277-786X/17/$18 · doi: 10.1117/12.2309215

ATHERMAL FIBER LASER FOR THE SWARM ABSOLUTE SCALAR MAGNETOMETER

W. Fourcault[1] & J-M. Léger[1], V. Costes[2], I. Fratter[2], L. Mondin[2]
[1]*CEA-LETI, MINATEC, 17 rue des Martyrs, 38054 Grenoble Cedex 9, France*
jean-michel.leger@cea.fr.
[2]*Centre National d'Etudes Spatiales, 18 Avenue Edouard Belin, 31401 Toulouse Cedex 9, France*

I. INTRODUCTION

The Absolute Scalar Magnetometer (ASM) developed by CEA-LETI/CNES is an optically pumped ^{4}He magnetic field sensor based on the Zeeman effect and an electronic magnetic resonance whose effects are amplified by a laser pumping process [1-2]. Consequently, the role of the laser is to pump the ^{4}He atoms at the D_0 transition as well as to allow the magnetic resonance signal detection.

The ASM will be the scalar magnetic reference instrument of the three ESA Swarm satellites to be launched in 2012 in order to carry out the best ever survey of the Earth magnetic field and its temporal evolution. The sensitivity and accuracy of this magnetometer based on ^{4}He optical pumping depend directly on the characteristics of its light source, which is the key sub-system of the sensor.

We describe in this paper the selected fiber laser architecture and its wavelength stabilization scheme. Its main performance in terms of spectral emission, optical power at 1083 nm and intensity noise characteristics in the frequency bands used for the operation of the magnetometer, are then presented. Environmental testing results (thermal vacuum cycling, vibrations, shocks and ageing) are also reported at the end of this paper.

II. FIBER LASER ARCHITECTURE

Given the role of the laser in the ASM instrument, the following specifications have to be met:

- Wavelength stability with piezoelectric modulation piezoelectric modulation around the D_0 transition : λ=1082.908 nm in air standard (std)
- Relative Intensity Noise (RIN) lower than -135 dB/√Hz at 1 kHz and 2 mW of output optical power
- Spectral linewidth lower than the D_0 absorption width of 1.7 GHz
- Specific space environment and space design requirements

A. Global laser architecture

As commonly seen, our fiber laser consists of a pump laser diode, a Wavelength Division Multiplexer (WDM), an Yb doped Fiber Bragg Grating (FBG), an optical isolator and a splitter to allow a feedback control.

In this architecture, the noise reduction loop acts on the pump diode current by detecting the low frequency fluctuations of the output optical power from the dedicated photodiode located in the 20 % splitter output.

The corresponding block diagram is presented in Fig. 1.

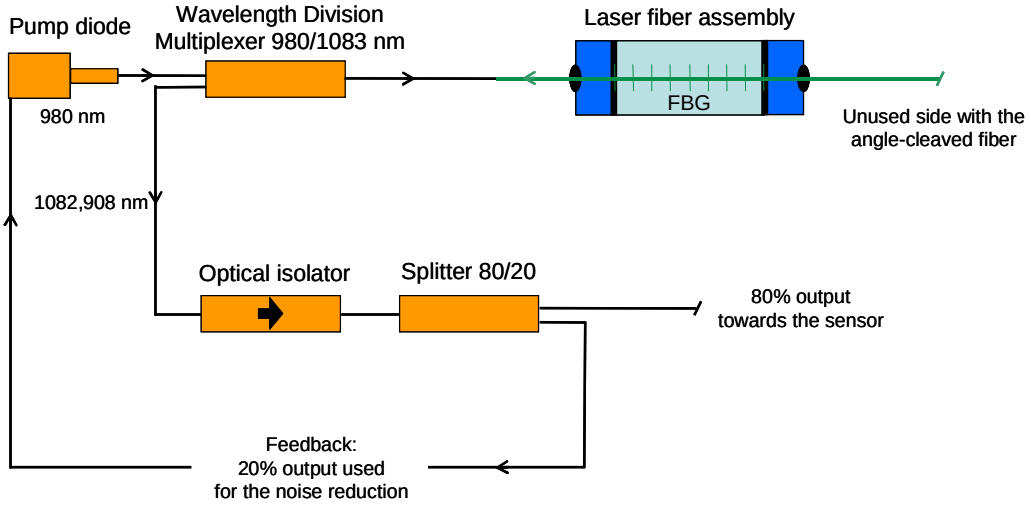

Fig. 1. Laser architecture

B. Athermal design of the Laser Fiber Assembly (LFA)

The ASM laser has to be able to pump the ^{4}He at 1082.908 nm (in air std) within the temperature range of [-5 °C; +50 °C] which is the specified qualification operating temperature range of the ASM electronics on the Swarm satellites. One of the main challenges to take up for the LFA conception was to reduce the thermal wavelength drift as much as possible in a passive way. We could have used, for example, a 1083 nm laser diode with a thermo-electric Peltier device but the laser consumption would have been highly increased.

In order to detail the achieved passive athermal LFA design we remind here first the theoretical principle behind the operation of the FBG. The reflected wavelength λ, also called the Bragg wavelength, is given by the following equation:

$$\lambda = 2n\Lambda \tag{1}$$

where *n* is the effective refractive index of the fiber and Λ is the grating period.

When differentiating this equation (and only considering the fluctuations due to the temperature), we obtain:

$$\frac{d\lambda}{\lambda \cdot dT} = \frac{dn}{n \cdot dT} + \frac{d\Lambda}{\Lambda \cdot dT} \tag{2}$$

The grating period Λ is modified by adapting the Bragg grating length L (which is in our case about 50 mm). Thus, we deduce:

$$\frac{d\lambda}{dT} = \lambda \cdot \frac{dn}{n \cdot dT} + 0.78 \cdot \lambda \cdot \frac{dL}{L \cdot dT} \tag{3}$$

where the 0.78 coefficient accounts for the photo-elastic effect of fiber.

Equation (3) describes the wavelength behavior with respect to the temperature. The first term is commonly called “thermo-optic constant” and is characteristic of the fiber (about +7 pm/°C for our Yb doped fiber). The second term corresponds to the thermal wavelength drift in relation to the fiber thermal expansion.

The aim of the athermal LFA design is to obtain a wavelength thermal drift close to 0 pm/°C by achieving the compensation of the first term by the second one in equation (3). Solving this equation has led to the final design where a global negative thermal expansion coefficient has been achieved due to a specific assembly of aluminium, titanium, Zerodur® (zero expansion glass-ceramic) pieces and a piezoelectric actuator. The role of the piezoelectric actuator (made by the CEDRAT Group) [3] is to modulate and to allow a fine tuning of the laser wavelength around the ^{4}He D_0 transition. A picture of the final LFA design is given in Fig. 2.

C. Fixation system

Another challenge to take up was the design of a suitable fixation system of the LFA allowing it to comply with the shocks and vibrations specifications. A solution has been developed using a titanium bridge**,** coned-disc springs (also known as Belleville washers) and elastomers (with suitable thickness and hardness, and a low outgassing characteristic).

The pieces of elastomer are located under the LFA and between the titanium bridge and the LFA in order to dampen any tri-axis vibrations or shocks. This fixation system has successfully passed the vibrations and shocks qualification tests. The final titanium fixation bridge is shown on the LFA of Fig. 2.

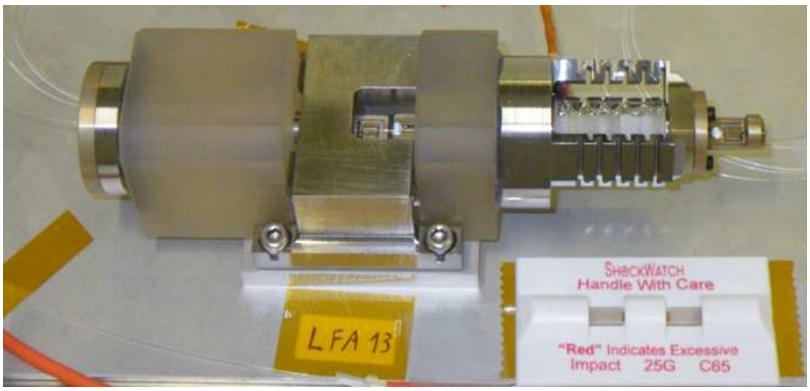

Fig. 2. Photography of a LFA: the pre-stressed piezoelectric actuator on the right is glued on the Zerodur®; the LFA is then fixed in the ASM electronics box with the titanium bridge put upon the Zerodur®

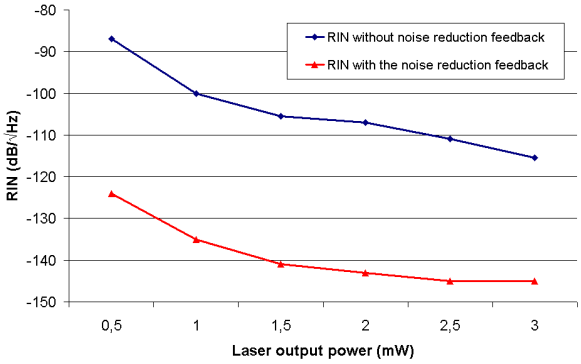

Fig. 3. RIN measured at 1 kHz with a SWARM flight model laser

IV. LASER PERFORMANCE

A. RIN performance

For both consumption and simplicity reasons, in the ASM instrument it has been chosen to detect the magnetic resonance signals coming from the ^{4}He cell around 1 kHz, which corresponds to the 1 kHz modulation of the continuous part of the LA0 magnetic resonance signals between the Zeeman sub-levels [4]. This signal is high enough to allow the measurement of the magnetic field with a low noise laser: the corresponding RIN measurement of the ASM laser is shown in Fig. 3 (obtained from an electronic spectrum analyzer and an InGaAs photodiode). As shown, the low frequency feedback control loop presents the opportunity to reduce the RIN from about -105 dB/√Hz at 2 mW of output power around 1 kHz down to -140 dB/√Hz. The low noise laser specifications are thus met.

B. Wavelength and power performance in thermal vacuum environment

Given that an active medium is present in the fiber laser (Yb doping), there are energy losses during the wavelength conversion. These thermal losses induce an increase of the local temperature which is amplified under vacuum conditions. Several tests have demonstrated that this increase of temperature make the laser unstable, the power drop and the wavelength rapidly increase even with low pump powers of about 10 mW and a fiber diameter of 250µm.

A suitable way to enhance the thermal dissipation and thus to properly operate the laser under vacuum was eventually found and implemented. In addition, this solution has allowed the reduction of the acoustic disruption as well as the improvement of power and wavelength performance. A few results are given in Fig. 4.

The first graph in Fig. 4 shows that this thermal dissipation solution increases the output power as well as reduces the wavelength fluctuations when the pump power is increased in air environment. The same results are obtained when this test is carried out under vacuum (with the thermal dissipation solution).

On the second graph in Fig. 4, the thermal wavelength drift of the LFA has been demonstrated lower than 1 pm/°C (typically close to 0.5 pm/°C) when operated over the qualification temperature range of [-5 °C; +50 °C].

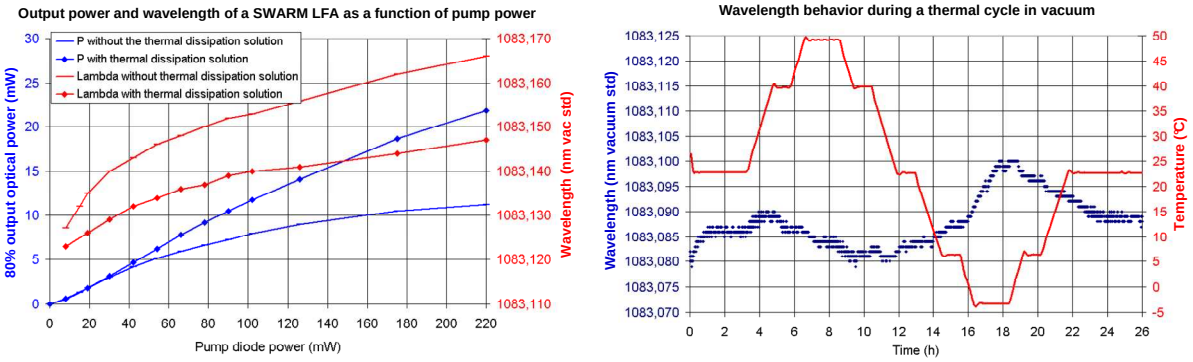

Fig. 4. Power and wavelength measurements with and without our thermal dissipation solution in air (on the left) and wavelength behavior during a thermal cycle in vacuum (on the right)

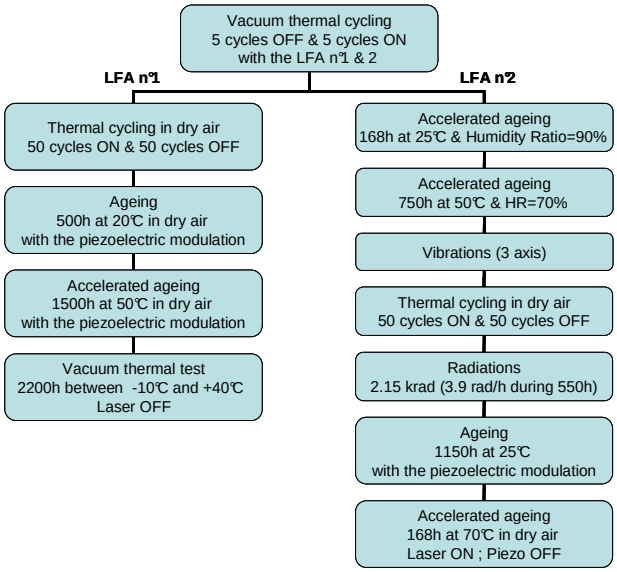

	Success criteria
Optical output power at 100 mW of pump power	> 2 mW
Optical power stability (during 1h)	< 0.5 dB
$\Delta\lambda$ measured during the piezoelectric activation (from 0 to +150 V)	> 210 pm
λ (in vacuum std) at 2 mW of output power, within [-5; +50] °C	$\in$ [1083.000;1083.200] nm
RIN at 1 kHz and 2 mW of output power	< -135 dB/√Hz
Visual inspection	No visible change

Fig. 5: Qualification test sequence applied to two LFAs (on the left) and corresponding success criteria used for the qualification (on the right)

IV. LFA QUALIFICATION TESTS

Before starting the qualification tests of the LFA itself, we had to pre-test a few of its sub-parts. We also had to qualify the gluings that are necessary to perform the LFA assembly. It eventually requires four different glues and two of them are structural.

To this end, we have simulated and tested several glues and geometries of gluing areas. The final glues and corresponding glues areas have been successfully obtained and tested with their dedicated processes which have been developed and applied in the collaboration with the NKT Photonics Company.

In addition to these pre-qualification tests, the LFA has successfully passed the qualification sequence described in Fig. 5 with the corresponding success criteria.

The thermal cycles that have been performed are [-5 °C; +50 °C] when the laser was ON and [-20 °C; +50 °C] when it was OFF. Performance tests have been carried out between every qualification tests (typically a visual inspection in addition to wavelength, optical power and stability measurements).

V. CONCLUSIONS

The CEA-LETI and the CNES have been able to develop an athermal laser fiber with enhanced performance in air as well as under vacuum conditions. It complies with all the specifications, and to our knowledge, such a laser will be the first to be flown in space.

Currently, the magnetic sensor including this laser has demonstrated a resolution lower than 1 pT/√Hz in the measurement range [15 µT; 65 µT] and is in full compliance with the requested metrological performance [2].

This type of laser could also be used for other applications such as atomic spectroscopy experiments.

REFERENCES

[1] C. Guttin, J.M. Léger and F. Stoeckel, "An isotropic earth field magnetometer using optical pumped helium 4", Journal de Physique IV, Colloque C4, supplément au Journal de Physique III, Volume 4, avril 1994, pp. C4-655-659.

[2] T. Jager, J-M. Léger, F. Bertrand, I. Fratter and J-C. Lalaurie, "SWARM Absolute Scalar Magnetometer accuracy: analyses and measurement results", IEEE sensors 2010 paper N° 1564, in press.

[3] T. Maillard, F. Claeyssen, R. LeLetty, O. Sosniki, A. Pages, "Piezo mechatronic based systems in aircraft space and defence applications", SPIE DSS – Space Exploration Technologies 2 – Session 4 – Support Technologies for Space Missions – 7331-20

[4] C. Cohen-Tannoudji, C., Théorie quantique du cycle de pompage optique. Vérification expérimentale des nouveaux effets prévus (Thèse d'Etat, Paris), Ann. Phys. Paris 7 p.423 and 469 (1962)